 doi:10.20944/preprints202206.0323.v1

Article

A Novel Triple Radar Arrangement for Level 2 ADAS Detection System in Autonomous Vehicles

Javad Enayati [1], Pedram Asef [1]* and Yeshwanth Jonnalagadda [1]

[1] Dept. Engineering and Technology, University of Hertfordshire, Hatfield, AL10 9AB, United Kingdom; j.enayati@herts.ac.uk; p.asef@herts.ac.uk; yj20aac@herts.ac.uk

* Correspondence: p.asef@herts.ac.uk; Tel.: +44(0)1707284691

Abstract: The main functions of the automated systems rely on the advanced sensors for detection and perception of the environment around the vehicle. Radars and cameras are commonly utilized to detect the potential obstacles and vehicles ahead on the road. Nevertheless, cameras can generate spurious detections in the extreme weather conditions such as fog, rain, dust, snow, dark, and heavy sunlight in the sky. Due to limitations in vertical field view of the radars, single radars are not reliable to detect the height of the targets precisely. In this paper, a triple radar arrangement (long-range, medium-range, and short-range radars) based on sensor fusion technique is proposed to detect objects with different size in level 2 Advanced Driver-Assistance (ADAS) system. The typical objects including truck, pedestrians, and animals are detected in different scenarios. The developed model considered ISO 26262 and ISO/PAS 21448 to reasonably address insufficient robustness and inability of the sensors. The models of sensor and level 2 ADAS systems are developed using MATLAB toolbox and Simulink. Sensor detection performance is determined by running simulations with triple radar setup. Obtained results demonstrate that the proposed approach generates accurate detections of targets in all tested scenarios.

Keywords: Autonomous vehicles, triple radar, Level 2 ADAS system, lane keeping assistance, nonlinear model predictive controller, safety, autonomous emergency braking.

1. Introduction

Developing automotive industry has brought about a competitive space for manufacturers to introduce safe, affordable, entirely self-sufficient vehicles [1]. This has led to a massive shift to a greater reliance on machines rather than people, necessitating a more intense design and research analysis of the advanced driver-assistance system (ADAS) [2]. After introducing the first semi-automated vehicle by Houdina Radio Control in 1926, lots of achievements have been obtained by related industries [3]. General Motors' Motorama car expo in 1960 unveiled a few automated vehicles (AVs) based on previous effective ideas [4]. Further, in the development of AV technology, some brilliant advancements in the EUREKA's Prometheus Project, and the Stanley automated vehicle have been obtained [5]. Authors in [6] show a clear picture of the three decades of ADAS technology developments. The SAE document J3016 202104 lays out the taxonomy for all six levels (level zero to level fifth) of ground vehicle driving automation. Adopting at least level 2 ADAS features in vehicles offer a significant increase in safety and emission reduction.

According to [7] a fully autonomous vehicle should be able to learn from its surroundings in real time to make decisions based on the perceptive view and local view. Automotive sensors are broadly applied to give real-time data to the AVs [8]. The Exteroceptive sensors which perceive the environment like radars, cameras, and lidars are the most important part of the measurement system [9,10]. Although cameras serve excellent visual results for objects around an AV, the weather conditions can significantly influence the reliability and robustness of detections. Authors in [11] suggested that a 3-

 doi:10.20944/preprints202206.0323.v1

level refinement of video-based data improves the detection when the video is at 55 fps. This approach uses different algorithms at each level to keep false detections as low as possible. There is a lot more room to improve in the motion algorithms and their likelihoods. A robust Adaboost detection algorithm capable of full and half body detections is utilized in [12] to improve vision detections using cameras. This method requires a high computation time as it applies multiple training samples with information about moving vehicles, pedestrians, and motorcyclists. In [13], the authors studied the challenges to build a multi-camera dataset for driver monitoring system is carried out. This work also describes the approach for handling the technical issues during the design and implementation of the monitoring systems.

Radars use considerably cheaper technology compared with cameras. While Millimeter-wave high-performance radars have an angular resolution of 1°, in [14] authors proposed a better wide aperture radar with angular resolution up to 0.1° which provides more precise detections in long range as compared to that of Lidars. Researchers in [15] conducted a study on developing high-resolution 4D sensing radar system for an autonomous vehicle using machine learning methods like the deep neural network (DNN) technique. The results approved that targets with low Radar cross section (RCS) are detected in the low sidelobes. Additionally, a novel low RCS radar with a diffraction mitigation technique is designed in [16] so that the Radar focus on highly vulnerable pedestrians and cyclist at the corners. Some researchers have proposed algorithmic procedures to enhance the accuracy of detection results obtained by Radars. In [17], the researchers compared the radar detection and ground truth data, an accuracy model for a radar system is developed. Then radar latency is obtained according to the relative velocity. Nevertheless, such a paradigm requires numerous tests on a specific detection system.

The efficiency of ADAS can be increased with the implementation of reinforcement learning in control strategies [18]. Several experiments in developing a decision-making strategy using deep reinforcement learning (DRL) are conducted in [19]. DDPG algorithm is utilized in conjunction with DRL to improve the efficiency of the autonomous emergency braking (AEB) system. Results demonstrate that in extreme scenarios like high speeds and very low distances between vehicles, the proposed algorithm failed to provide passenger comfort and mitigate the collision. Then, further investigation using multi-agent reinforcement learning was proposed. A lane keep assist (LKA) system is designed in [20] that can transition between lane departure prevention and lane keep co-pilot modes. This method uses a model predictive control scheme and an extended Kalman filter for learning the dynamics. The whole system is modelled in Simulink. The model is integrated into the CarSim to test the performance of the assist modes using driver-in-the-loop testing. The system achieved switchable modes with 90% accuracy without violating the vehicle dynamics. However, the proposed approach requires embedded processors with high computational resources. Researchers in [21] adopted a Takagi-Sugeno (T-S) fuzzy-based robust H∞ algorithm in development of LKA system. This approach considers the uncertainties, disturbances, and longitudinal velocities for robust control of desired steering input. To overcome the varying shadows and occlusions, an approach based on the model of lane boundaries in 3D-space is developed in [22]. This method also applies color information for effective clustering to remove the outlier and estimate the curvature. Despite acceptable results, the processing system requires high computational resources.

This work aims to develop a level 2 driving automation with a reliable and robust object detection system. A triple radar setup based on long-range, medium-range and short-range radars is developed to detect objects with different heights, sizes, distances, and velocities. Since level 2 ADAS requires longitudinal and lateral control assistance for the driver, hence, the AEB and LKA systems are developed and integrated into the model. For reliable detections purpose, a global nearest neighbor (GNN) combined with extended Kalman filter (EKF) algorithms are used to generate tracks for multiple objects which are utilized to find the relative distance and velocity of targets. To test the modeled

Preprints (www.preprints.org) | NOT PEER-REVIEWED | Posted: 23 June 2022 doi:10.20944/preprints202206.0323.v1

subsystems and final level 2 ADAS system, different simulations are conducted using MATLAB toolboxes and Simulink. Obtained results demonstrate that the proposed approach generates accurate detections of moving targets in all tested scenarios.

2. Developed Framework

The main goal of an AV is to provide a safe and efficient transportation between initial and final states without any human intervention. In this work, perception and decision-making systems are applied as major functions in the AV's framework. The perception system utilizes the measurements from exteroceptive sensors to calculate the AVs' dynamic parameters and detect other objects in the environment. The measurement setup includes radars and cameras. Dynamic parameters are mostly internal states of the vehicle, therefore, estimation paradigms are used to estimate the desired states. The decision-making function acts on the LKA, AEB and adaptive cruise control (ACC) algorithms to fulfill requirements of the multi-stage collision avoidance system. A model predictive controller (MPC) is employed to create the necessary control actions. The developed framework for the studied AV is shown in Figure 1. In this framework, the proposed triple radar sensors with short, medium, and long-ranges (SR, MR, and LR) offered more reliability and robustness in the detection system. The multi-range radar system observes and generates a forward collision warning (FCW) followed by a multi-stage autonomous collision avoidance breaking (MSCA) to safely apply brake considering the lead object (LO) which can be a moving or constant obstacle such as a pet, cyclist, vehicle, etc. Based on ISO 26262 series and ISO/PAS 21448, the sensor's functionality and

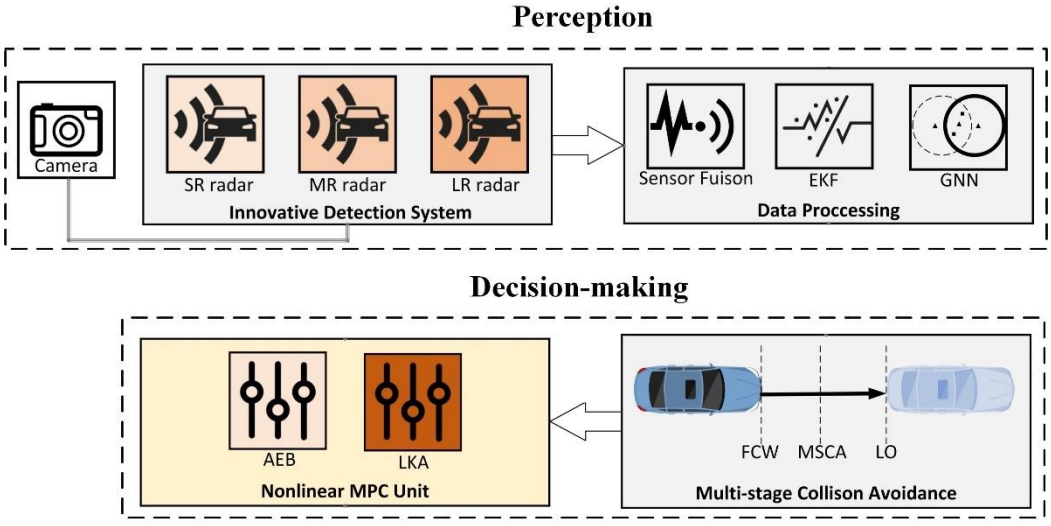

Figure 1. Developed framework for the studied AV.

limitations are studied under different environmental conditions.

3. Simulation Methodology

MATLAB tools are utilized to develop the Level 2 autonomous vehicle system with a triple radar arrangement for reliable detections. A high-level closed-loop system design architecture with four main subsystems is developed in MATLAB Simulink environment, presented in Figure 2. The perception subsystem uses sensors and sensor fusion techniques to understand the environment and road information around an ego vehicle. This block also contains the scenario builder. The AEB controller subsystem takes vehicle information, feeds the AEB control logic which is written using state flow and produces the deceleration forces. Road information is used in the LKA controller subsystem to find the road curvatures. To regulate the movement of the ego vehicle, the outputs of the control signals from both AEB and LKA are supplied to the vehicle dynamics block. The vehicle dynamics block outputs the coordinate details of the ego vehicle at each time step and sent them as an input to the perception block.

Preprints (www.preprints.org) | NOT PEER-REVIEWED | Posted: 23 June 2022 doi:10.20944/preprints202206.0323.v1

3.1. Perception

In the carried-out simulations, functions of the perception block are as follows:

3.1.1. Scenario builder

Scenarios are created using Driving Scenario Designer application available in automated driving toolbox. This application helps to create synthetic scenarios to test the autonomous driving systems. Road networks are designed to host the different actors, traffics signs, and relative trajectories. Driving Scenario Designer also gives flexibility of configuring the sensor parameters to replicate the real sensors.

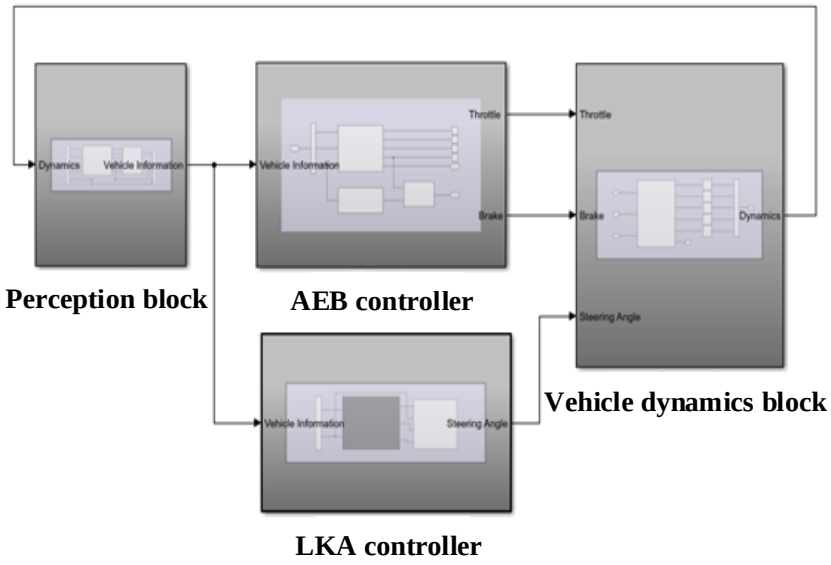

Figure 2. Simulation architecture.

3.1.2. Radar

Radars quantify the relative position and velocity of obstacles using emitted electromagnetic wave travel time and the Doppler feature, respectively. They send out continuous chirps which are generated by a frequency synthesizer at the desired frequency. The waves are amplified based on the defined coverage and range. Amplified signals are then converted to electromagnetic waves by a transmission antenna. The reflected signal is captured by the receiver antenna and passed through a low noise filter. Then, it is mixed with the transmitted signal to generate the beat frequency signal. The beat frequency signal is converted to digital and processed using a signal processor to extract range and velocity information of detections. Following are principal equations to extract the relative range and velocity:

$$R = \frac{11 * d_{res} * R_{max} * f_b}{\mathrm{c}} \quad (1)$$

$$\vartheta = 0.5 * \lambda * \Delta f \quad (2)$$

where, R and ϑ are the target range and velocity, c is the speed of light, f_b is the beat frequency, R_{max} and d_{res} are maximum range and range resolution of radar, respectively. The λ is the wavelength and the Δf is the Doppler frequency shift. In this study, three radars (long-range, medium-range, and short-range radars) are used in a level 2 ADAS system to sense the environment in front of the vehicle in both highway and urban driving scenarios. The applied radars with reported specifications in Table 1 are arranged such that detect objects of different sizes and velocities.

Table 1. Specifications of the applied radars.

Preprints (www.preprints.org) | NOT PEER-REVIEWED | Posted: 23 June 2022 doi:10.20944/preprints202206.0323.v1

Radar type	Mounting height (m)	Range (m)	Azimuth FoV	Vertical FoV
Short-range radar	0.2	60	120°	1°
Medium-range radar	1.2	90	60°	1°
Long-range radar	0.8	120	30°	1°

3.1.3. Camera

A camera detects light emitted from the environment on a photosensitive surface (image plane) using a lens to take photograph [23]. Cameras are inexpensive with the capability of detecting both moving and motionless objects in their field of vision (FoV), as well as provide high-resolution photos of their surroundings. However, the probability of producing accurate moving target detections in bad weather conditions and environments is very low, and non-moving targets detection like lane boundaries are given importance from vision detection point of view. Hence, the camera is used only for lane detection in the proposed detection system. The main characteristics of the applied camera, in this paper, is shown in Table 2.

Table 2. Specifications of the applied camera.

Camera intrinsic	Values	Camera parameters	Values
Focal length X (px)	800	FoV	100°
Focal length Y (px)	800	Range (m)	75
Image width (px)	2000	Mounting height (m)	1.1
Image height (px)	480	Pitch angle	1°
Principle point X pixel	320		
Principle point Y pixel	240		

3.1.4. Sensor fusion

To reduce uncertainty in AV operations, implemented algorithms aggregate and combine data from numerous sensors. Sensor fusion algorithms contain data gathering, calibration and clustering functions. In this work, the data received from radars and camera sensors are brought to a common reference plane for preprocess calibration [24]. Reference point on a vehicle, sometimes can be center of gravity (CoG) of the vehicle. As dynamics and lateral control of the vehicle are also considered in this work, front axle center is considered as reference point. Also, based on radars resolution in azimuthal plane and vehicle size, several detections from single object are captured by radars.

3.1.5. Multi Object Tracking (MOT)

MOT creates, confirms, predicts, corrects, and deletes moving object tracks. Detection reports generated by sensors are given as inputs to the multi-object tracker. Using the GNN criterion, the MOT system allocates the detection to a track. If the detection cannot be assigned to an existing track, the tracker creates a new one depending on assignment threshold attribute. When a tentative track receives enough detections, its status is changed to confirmed. If no detections are added to the track during a specific number of updates, it is deleted. The estimation paradigms are applied to generate the optimal tracks [25,26]. Methods in the literature mostly apply various forms of the Kalman Filter (KF) which is a fundamental tool for analyzing and solving a broad class of estimation problems [27]. In this work, the tracker estimates the state and state error for each track using an EKF algorithm. The states are applied to predict where a track will be in each frame, and how likely each detection will be assigned to that track.

3.2. AEB system

AEB system is the most beneficial and efficient ADAS system for passenger and target safety [28]. The AEB acts automatically when the space between the driver and the

Preprints (www.preprints.org) | NOT PEER-REVIEWED | Posted: 23 June 2022 doi:10.20944/preprints202206.0323.v1

hazard decreases, and the driver does not respond the hazard in time. In the conducted simulations, relative distance and velocity from perception block, and longitudinal velocity of vehicle from vehicle dynamics block are fed to AEB controller to calculate the important parameters such as time to collision (TTC) and stopping time. The logic for multistage braking with different deceleration values are built based on these parameters.

3.2.1. TTC

Time to collision (TTC) is calculated in seconds based on a predefined constant headway offset H_{offset} value in meters, relative distance $D_{relative}$, and relative velocity $V_{relative}$ as follows:

$$TTC = \frac{D_{relative} - H_{offset}}{V_{relative}} \quad (3)$$

When the TTC value is less than forward collision warning time T_{FCW}, the alert is triggered and AEB acts. T_{FCW} is calculated based on stopping time (the time period at which the ego vehicle initially applies the brakes until it comes to a complete stop) and reaction time of the driver T_{react}. The stopping time T_{stop} of a vehicle depends on the velocity of the vehicle v_{ego}, and brake deceleration a_b:

$$T_{FCW} = T_{react} + T_{stop} \quad (4)$$

$$T_{stop} = \frac{v_{ego}}{a_b} \quad (5)$$

The AEB system applies the brakes based on driver's comfort and vehicle dynamics. In this work, the brake decelerations are selected in three steps given as 3.8 m/s², 5.3 m/s², and 9.8 m/s².

3.2.2. AEB logic

AEB logic is created using state flow toolbox to make time dependent decision on T_{FCW} and three stages of braking. The selected AEB logics are as follows:

1. If the $TTC \leq 1.2 \times T_{FCW}$, forward collision warning is activated otherwise, AEB would be in the default mode.

2. If the $TTC \leq T_{FCW} @ a_b = 3.8$, brake deceleration is set to 3.8 m/s². When $v_{ego} \leq 0.1$, the AEB becomes deactivated.

3. If the $TTC \leq T_{FCW} @ a_b = 5.3$, brake deceleration is set to 5.3 m/s². When $v_{ego} \leq 0.1$, the AEB becomes deactivated.

4. If the $TTC \leq T_{FCW} @ a_b = 9.8$, brake deceleration is set to 9.8 m/s². when $v_{ego} \leq 0.1$, the AEB becomes deactivated.

3.3. LKA system

The LKA system, as a preventive ADAS, has high performance in averting the collisions which has root in moving out of the lane. LKA applies cameras for detecting lane markings and sidelines to direct the car using steering torques, as discussed in [29]. As the first LKA technology became accessible, many experiments were done to enhance LKA performance using various controller methods. Dynamic state feedback, layered PID, nonlinear MPC, and the use of an EKF have all been employed to improve lane maintaining performance [30]. The LKA algorithm and subsystem, applied in this work, are explained further in the following subsections.

3.3.1. Lane center estimation

The estimating lane center system sends data from lane sensors to the lane-keeping controller. A clothoid curve model is utilized to depict the barriers in which the curvature grows linearly with increasing distance. The previewed curvature provides the ahead curvature midline. In this work, the ego vehicle's calculations are done three seconds ahead. This look-ahead period allows the controller to use previewed data to compute the car's steering angle, which improves the MPC controller's efficiency.

Preprints (www.preprints.org) | NOT PEER-REVIEWED | Posted: 23 June 2022 doi:10.20944/preprints202206.0323.v1

3.3.2. Lane keeping controller

The MPC is integrated in the line keeping algorithm, in which its principles are discussed in this subsection. Considering the state vector X, in discrete time k+1, is predicted by:

$$X_{k+1,t} = \mathrm{A}.X_{k,t} + \mathrm{B}.U_{k,t} \tag{6}$$

where, $U_{k,t}$ is the control input. Given the length of the prediction horizon, N, the MPC minimizes the cost function J in equation (7):

$$J(X_t, U_t) = \sum_{k=1}^{N} (W_X \|X_{k,t}\|^2 + W_U \|U_{k,t}\|^2) \tag{7}$$

W_X and W_U are tuning weights which are set according to the requirements. Following equation is applied to determine the weights:

$$W_X = \sqrt{1 - W_U^2} \tag{8}$$

The controller behavior is further explored in terms of different W_X values is demonstrated in Figure 3.

In this work, $W_X = 0.2$ is selected for the utilized MPC controller. This value gives an acceptable compromise between accuracy and stability of the controller. When the MPC is applied in the LKA block of an ego vehicle, following matrices are defined:

$$A = \begin{bmatrix} -\frac{2(C_F + C_R)}{mV_X} & -V_X - \frac{2(C_F L_F - C_R L_R)}{mV_X} \\ -\frac{2(C_F L_F - C_R L_R)}{I_Z V_X} & -\frac{2(C_F L_F^2 - C_R L_R^2)}{I_Z V_X} \end{bmatrix} \tag{9}$$

$$B = 2C_F \begin{bmatrix} 1/m \\ L_F/I_Z \end{bmatrix} \tag{10}$$

where, m is the total vehicle mass, I_Z is the yaw moment of inertia of the vehicle, L_F is the longitudinal distance from the center of gravity to the front tires, L_R is the longitudinal distance from center of gravity to the rear tires, C_F is the cornering stiffness of the front

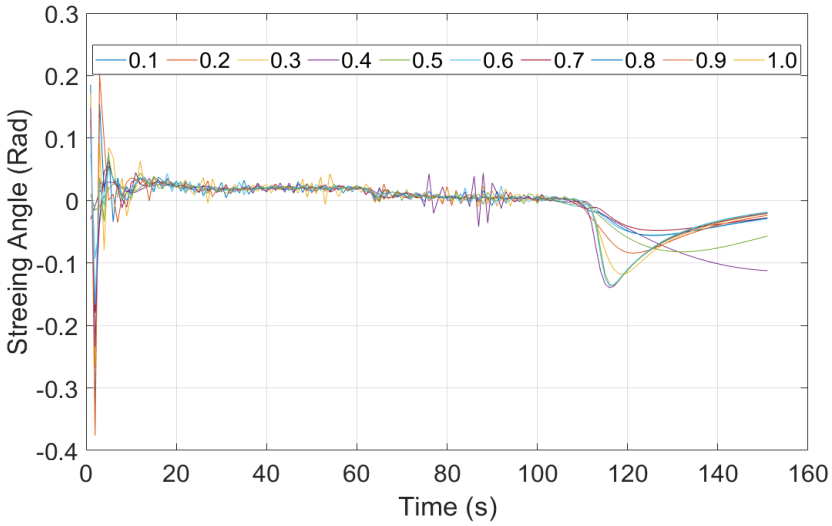

Figure 3. The weight effect on the MPC behavior.

tires, C_R is the cornering stiffness of the rear tires, and V_X is the longitudinal velocity of the ego vehicle.

Preprints (www.preprints.org) | NOT PEER-REVIEWED | Posted: 23 June 2022 doi:10.20944/preprints202206.0323.v1

The controller aims to manage the front steering angle to keep the vehicle in its lane and follow the curved road. The inputs for the controller are previewed curvature, longitudinal velocity, lateral deviation, and relative yaw angle. As shown in Figure 4, the steering angle is controlled by keeping the lateral deviation and relative yaw angle as low as possible. The steering angle is considered in the range of [-0.5, 0.5] rad due to the physical limits of the ego vehicle.

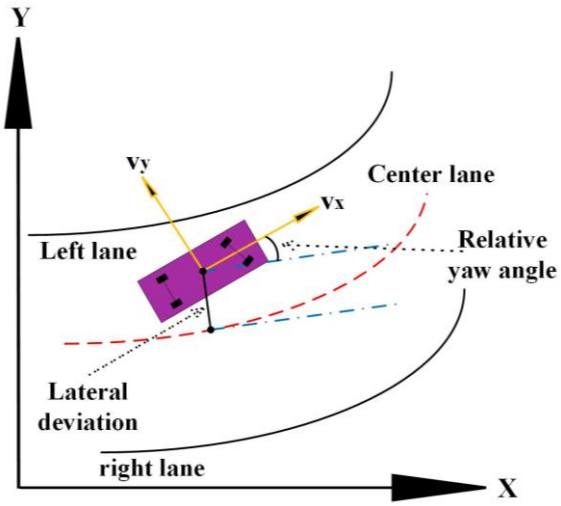

Figure 4. Lane keeping operation.

3.4. Vehicle dynamics

This block applies a 3-DoF equations to calculate the longitudinal, lateral, and yaw motions using a rigid two-axle vehicle body model. Body mass, aerodynamic drag, and weight distribution between axles due to the acceleration and steering are all considered in the block. The instant changes in the motions of the vehicle are calculated based on acceleration or throttle value, deceleration and/or brake value, and steering angle received from the controller. The vehicle dynamics block outputs the coordinate details of the vehicle at each time step and sent them as inputs to the perception block to feed the scenario builder part.

4. Simulation Results

The simulation results and performance testing of all the systems involved in this work are presented in this section. The simulations are carried out using MATLAB version R2021a with the computational resource at the University of Hertfordshire. A set of simulations as follows are done to validate the performance of the proposed level 2 ADAS:

1. Radar detection testing
2. AEB performance testing
3. LKA performance testing
4. Level 2 ADAS testing

The results including analytical and numerical graphs are explained in further detail in the following subsections.

4.1. Radar detection tests

Long-range radar is widely used for highway driving to assist AEB and LKA systems. To further improve the performance of the system, medium and short ranges radars are considered to enhance the capability of the proposed model in urban driving. Wide field view of short-range radar helps to detect the pedestrians attempting to crossing the street, running animals, occluded target behind the parked cars etc.

4.1.1. Animal detection

Preprints (www.preprints.org) | NOT PEER-REVIEWED | Posted: 23 June 2022 doi:10.20944/preprints202206.0323.v1

The bird's eye plot in Figure 5 (a) presents the animal crossing the road in front of the ego vehicle. The animal's height and length are both set to 0.4m. The target is initially located at a 30m horizontal distance and 40° FoV. The peaks of the short-range radar detections, in Figure 5 (b), demonstrate that multiple detections are generated at a certain time step as the object is moving perpendicular to the vehicle. Since the long and medium-range radars with 1° vertical FoV are located at 0.8m and 1.2m respectively, they are unable to detect the animal. Because of the detection complexities related to the dimension of the animals, adopting the wide view radars with low height results in a more reliable detection system.

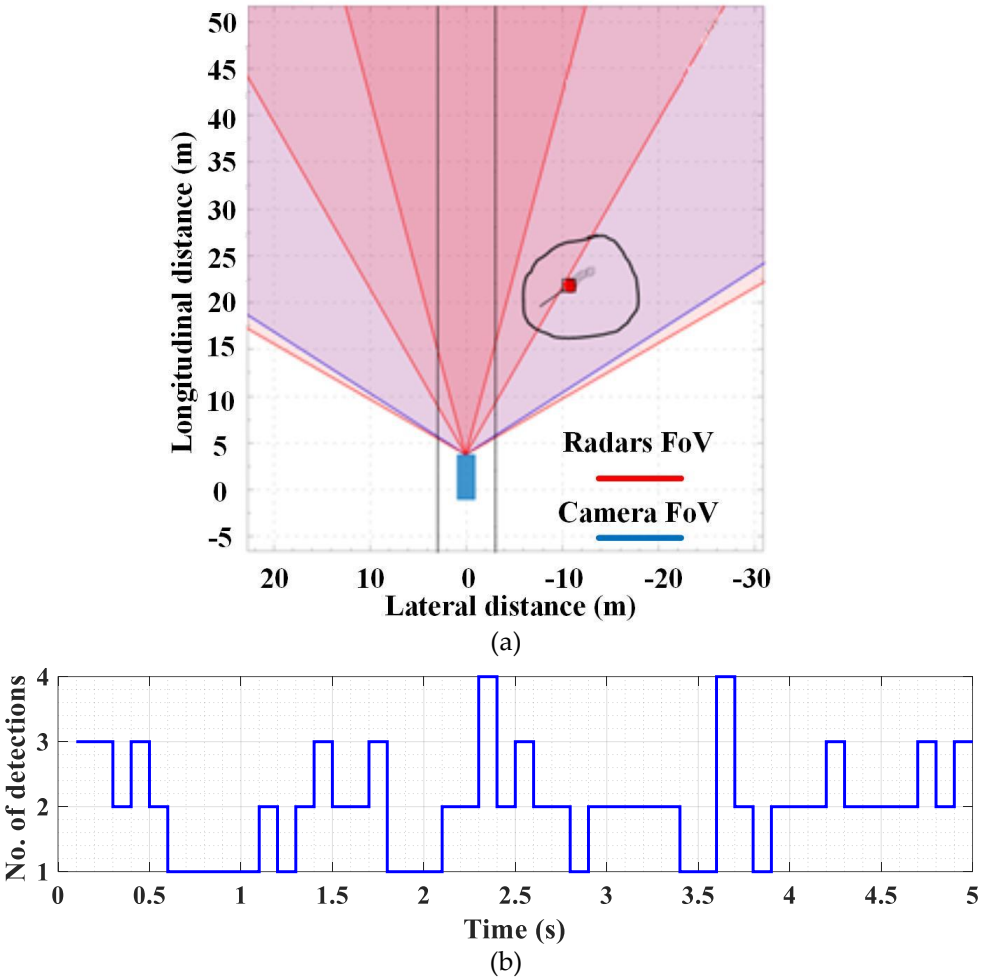

Figure 5. Results of radar setup performance in animal detection testing, (a) coordination in eye plot, (b) number of detections.

4.1.2. Pedestrian detection

In this test, a running pedestrian with a height of 1.5m crosses the road from the right side to the left side of the road. The velocity of ego vehicle and pedestrian is both selected 4m/s. The detection plots from the radars are shown in Figure 6. The short-range radar

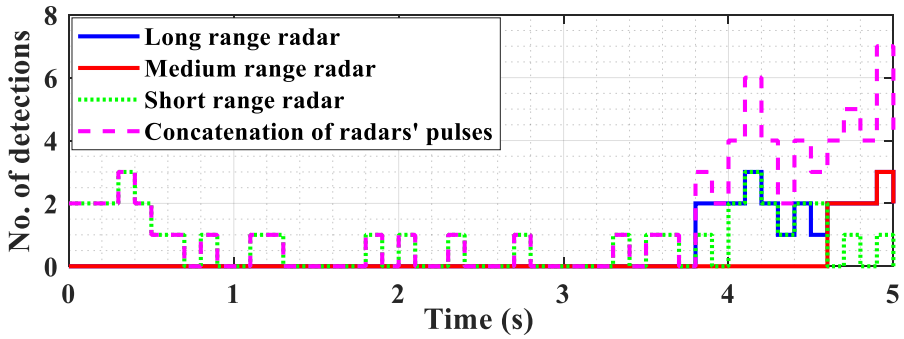

Preprints (www.preprints.org) | NOT PEER-REVIEWED | Posted: 23 June 2022 doi:10.20944/preprints202206.0323.v1

produced the fastest detection as it has the highest field of view. The medium and long-range radars have started generating the detections once pedestrian comes into 60° and 30° fields of view. As presented, after 3.8s the system has double detections and triple detection happens after 4.6s. Such a plan serves reliable output even in case of false detections of one radar. Concatenation of radar pulses is also shown in Figure 6 to show the detection pulse in the designed test.

Figure 6. Number of detections in radar pedestrian detection testing.

4.2. AEB performance tests

The performance of the AEB system is tested by applying three test scenarios created using a driving scenario designer with a 0.1s sample time. The proposed triple radar arrangement provides detections for the defined scenarios. The results of the conducted tests are explained in the following subsections.

4.2.1. Urban traffic scenario

In this scenario, a half-parked vehicle on a footpath is pulling out in front of the ego vehicle and stops at the center of the road. The velocity of the car and ego vehicle is constant at 3m/s and 10m/s respectively, and their initial distance is 70m. The scenario is run as depicted in Figure 7 (a). Based on the logic presented in the methodology section (subsection B.2) at 4.5s, the system recognizes that the TTC value enters logic 2, and a deceleration value of 3.8m/s^2 is applied then, the ego vehicle comes to halt at 7.7 sec. Figure 7 (b) clearly illustrates that the collision is avoided safely.

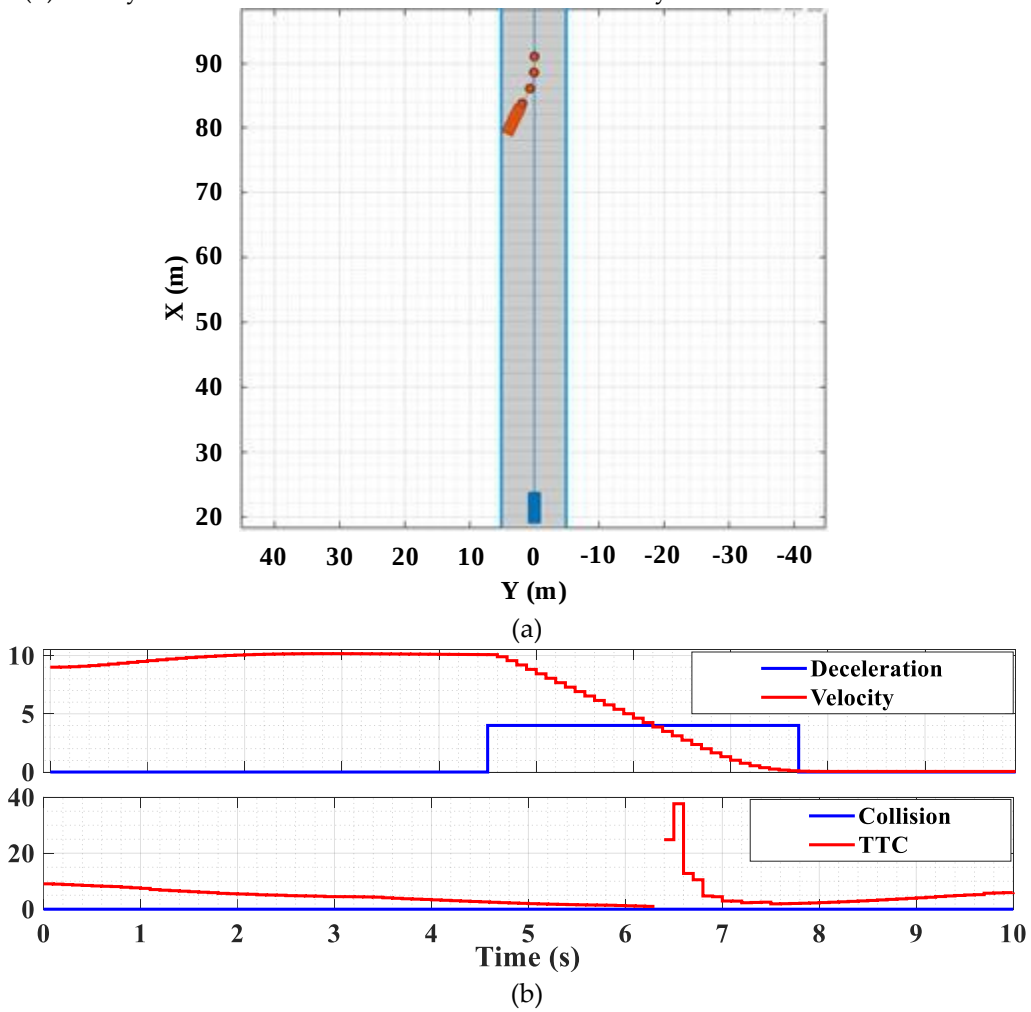

Figure 7. Results of AEB performance testing in urban traffic scenario, (a) coordination, (b) control parameters.

4.2.2. Motorway traffic scenario

Preprints (www.preprints.org) | NOT PEER-REVIEWED | Posted: 23 June 2022 doi:10.20944/preprints202206.0323.v1

In this scenario, a travelling truck at 25m/s goes out of the vehicle lane and comes back with a sharp steering angle. It completely comes to halt in the middle of the road with 90° yaw angle. The ego vehicle's velocity is 30m/s, and the initial distance is 180m. The truck is detected by long-range radar. The TTC initially enters the logic 2 at 5.4s, and the velocity of the ego vehicle is decreased with a deceleration of 3.8m/s². Nevertheless, at 5.5s the TTC value comes into the logic 3 and deceleration of 5.3m/s² is exerted on the ego vehicle. Figure 8 demonstrates that the system has satisfactory operation to avoid collision.

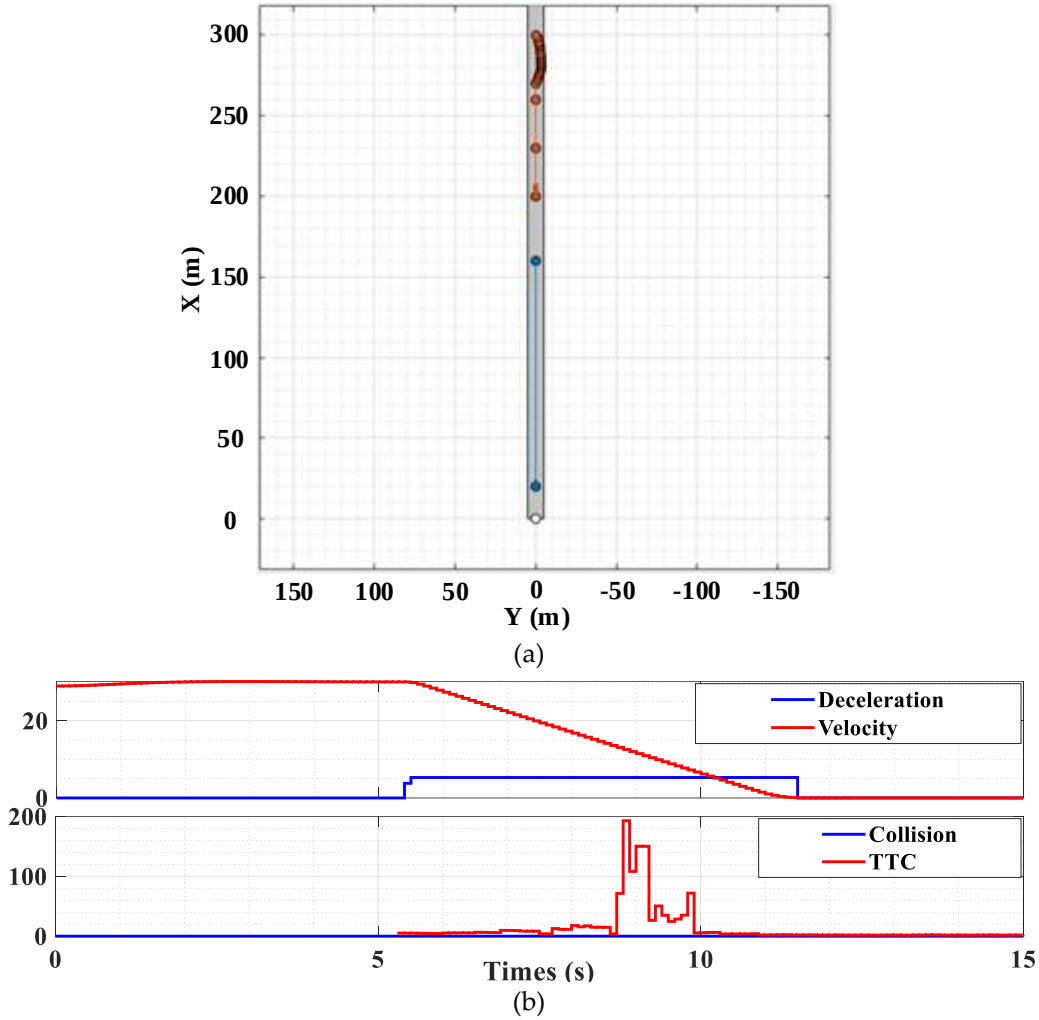

Figure 8. Results of AEB performance testing in motorway traffic scenario, (a) coordination, (b) control parameters.

4.2.3. Bicyclist in ego lane

This urban traffic scenario simulates the Euro NCAP testing scene bicyclist travelling forward in ego car lane at 4.17m/s. Ego car set velocity is 6.94m/s and the initial gap distance is 31m. If ego travels at the same velocity and collides with the bicyclist, the impact will be at the middle of the front bumper. The result presents that the logic 1 is activated at 4.7s. Based on the standard scenario, the cyclist increased the speed after 0.8s and the AEB does not enter the logic 2. However, at 6.4s ego vehicle comes close to the cyclist and the logic 2 is activated. The TTC forces the logic 3 to be activated at 6.5s and TTC values deceleration is increased to the 5.3m/s². The whole scenario is reported in Figure 9.

Preprints (www.preprints.org) | NOT PEER-REVIEWED | Posted: 23 June 2022 doi:10.20944/preprints202206.0323.v1

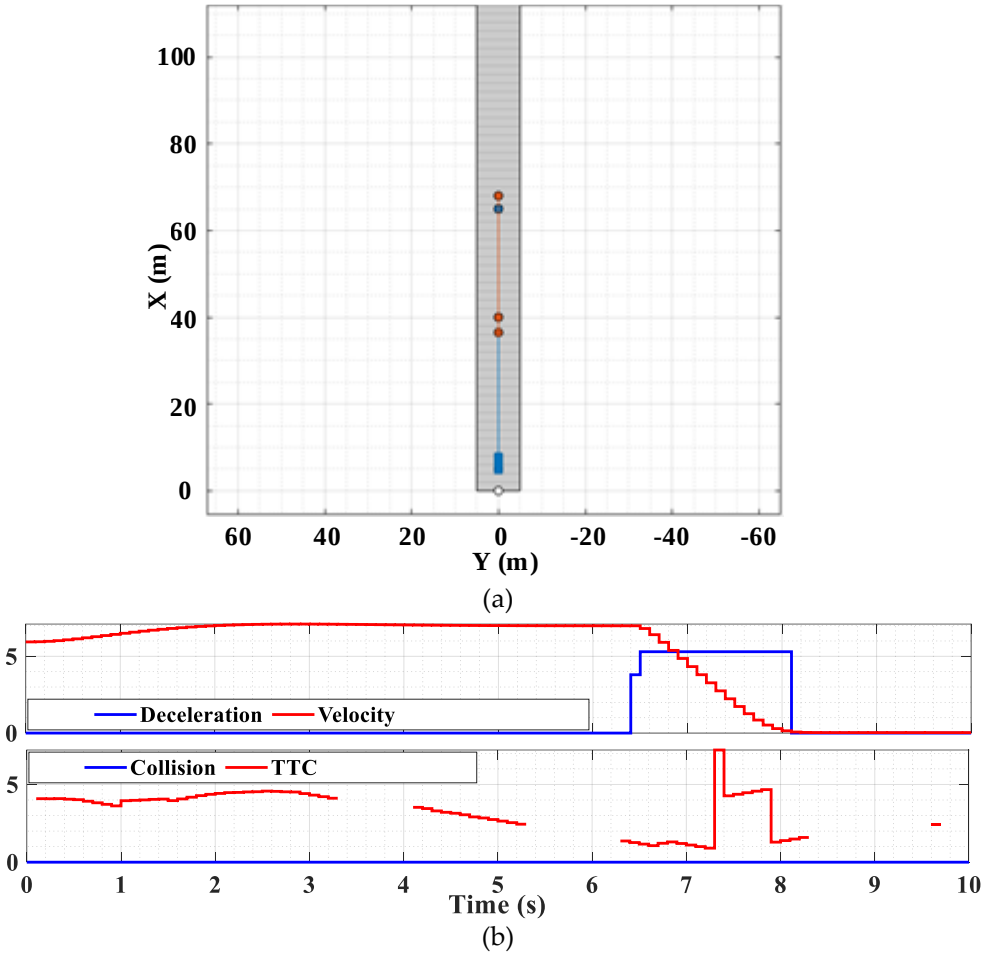

Figure 9. Results of AEB performance testing in Bicyclist in ego lane scenario, (a) coordination, (b) control parameters.

4.3. LKA performance tests

A LKA system utilizes the camera to detect the road lanes of different marking styles and colors. Although camera module can generate both lanes and objects, there is already a more reliable radar system for object detections. Therefore, the camera object detections are removed from the model which also saves the simulation times. To test the lane detections using LKA, two scenarios are created as follows:

4.3.1. Middle lane driving with white dashed markings on both sides

The bird's eye plot, presented in Figure 10 (a), shows that both lane boundaries are detected by the camera module. Using the left and right lane boundaries, the center lane is generated. Although the dashed markings are applied for this simulation, the camera predicts the center line accurately. The control parameters, in Figure 10 (b), demonstrate the performance of the LKA block in keeping the vehicle in the center lane.

Preprints (www.preprints.org) | NOT PEER-REVIEWED | Posted: 23 June 2022 doi:10.20944/preprints202206.0323.v1

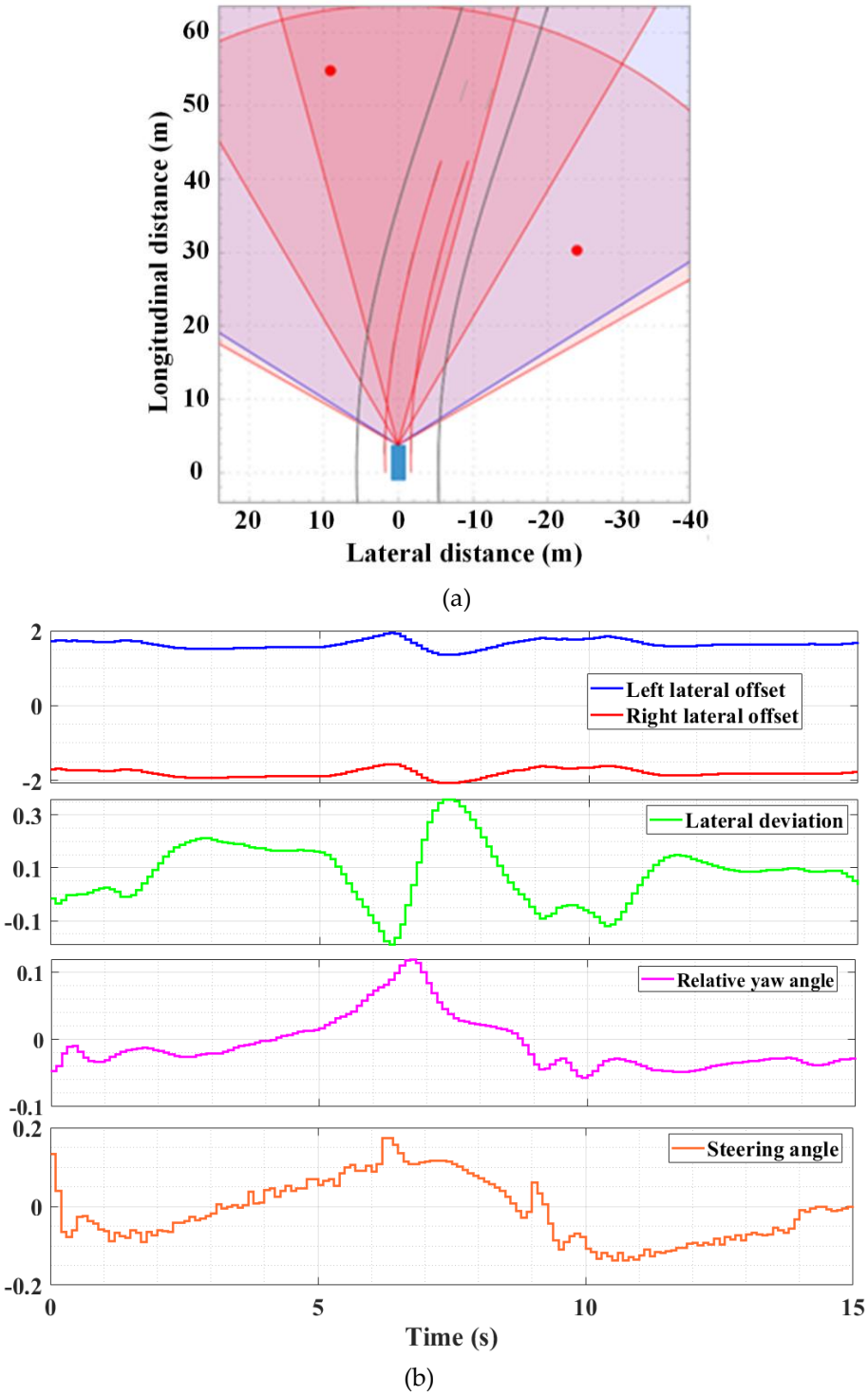

Figure 10. LKA performance in test with white dashed markings on both sides, (a) coordination in eye plot, (b) control parameters

4.3.2. Left lane driving with double solid yellow line on left and no marking on right

To put the maximum stress on the LKA system, the ego vehicle drives on the left lane while there are only double solid yellow lines on the left and no marking on right. The bird's eye plot, in Figure 11 (a), presents the lane boundary detections from the camera module. As presented, three seconds ahead curvature lanes boundary information is predicted only for the left side. The LKA predicts the curvature, curvature derivative, lateral deviation, relative yaw angle, and longitudinal velocity in the center lane using only single lane boundary information. These parameters are fed to the MPC controller

Preprints (www.preprints.org) | NOT PEER-REVIEWED | Posted: 23 June 2022 doi:10.20944/preprints202206.0323.v1

and a steering angle is generated to keep the car in the lane. The boundary for the steering angle is set to [-0.5 0.5] rad. Figure 11 (b) clearly illustrates that the steering angle has kept the limits.

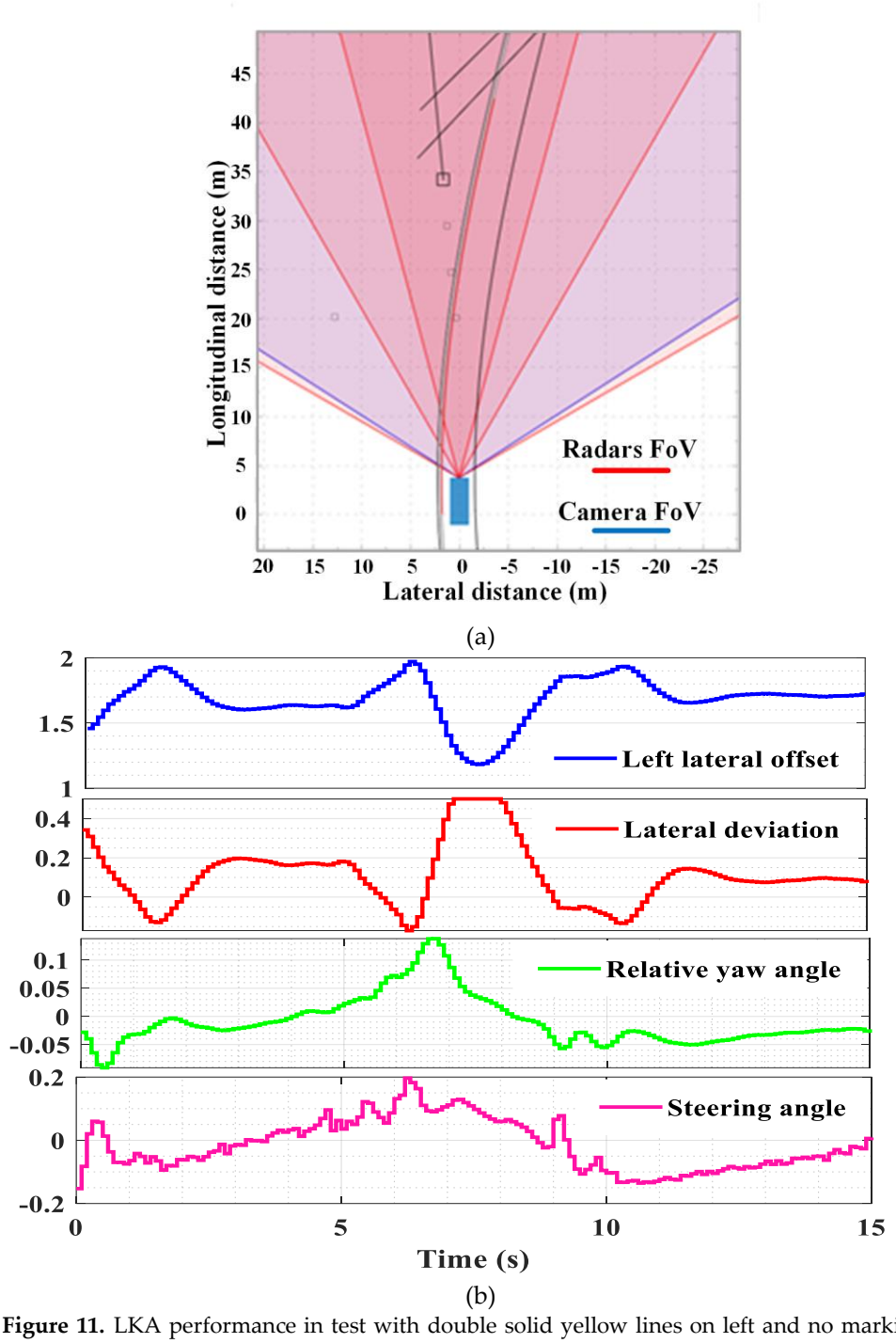

Figure 11. LKA performance in test with double solid yellow lines on left and no marking on right, (a) coordination in eye plot, (b) control parameters.

4.4. Level 2 ADAS testing

To test the performance of the proposed detection arrangement in the level 2 ADAS system, both AEB and LKA controllers in a highway scenario with two lanes are considered. Multiple actors, as reported in Table 3, are used in this scenario. Ego vehicles have 25m/s constant velocity. The arrangement of different vehicles is shown in Figure 12 (a). The selected highway has a circular shape with a radius of 500m. A positive steering angle is applied to keep the vehicle in the left lane. The triple radar setup is applied to detect the objects on the highway. Despite the existence of multiple actors, the proposed detection system identifies actor 1 which is in the same lane and closest to the ego vehicle as the most

Preprints (www.preprints.org) | NOT PEER-REVIEWED | Posted: 23 June 2022 doi:10.20944/preprints202206.0323.v1

important object. Based on the detected object, the TTC enters logic 2 at 5.9s. Due to the high velocity of the vehicle, the logic 2 is insufficient to avoid the collision. Therefore, the logic 3 is activated at 6s, and vehicle velocity is drastically reduced. At 10s the vehicle comes to a complete halt fully avoiding the crash. The control parameters, in Figure 12 (b), demonstrates the performance of the whole system in collision avoidance.

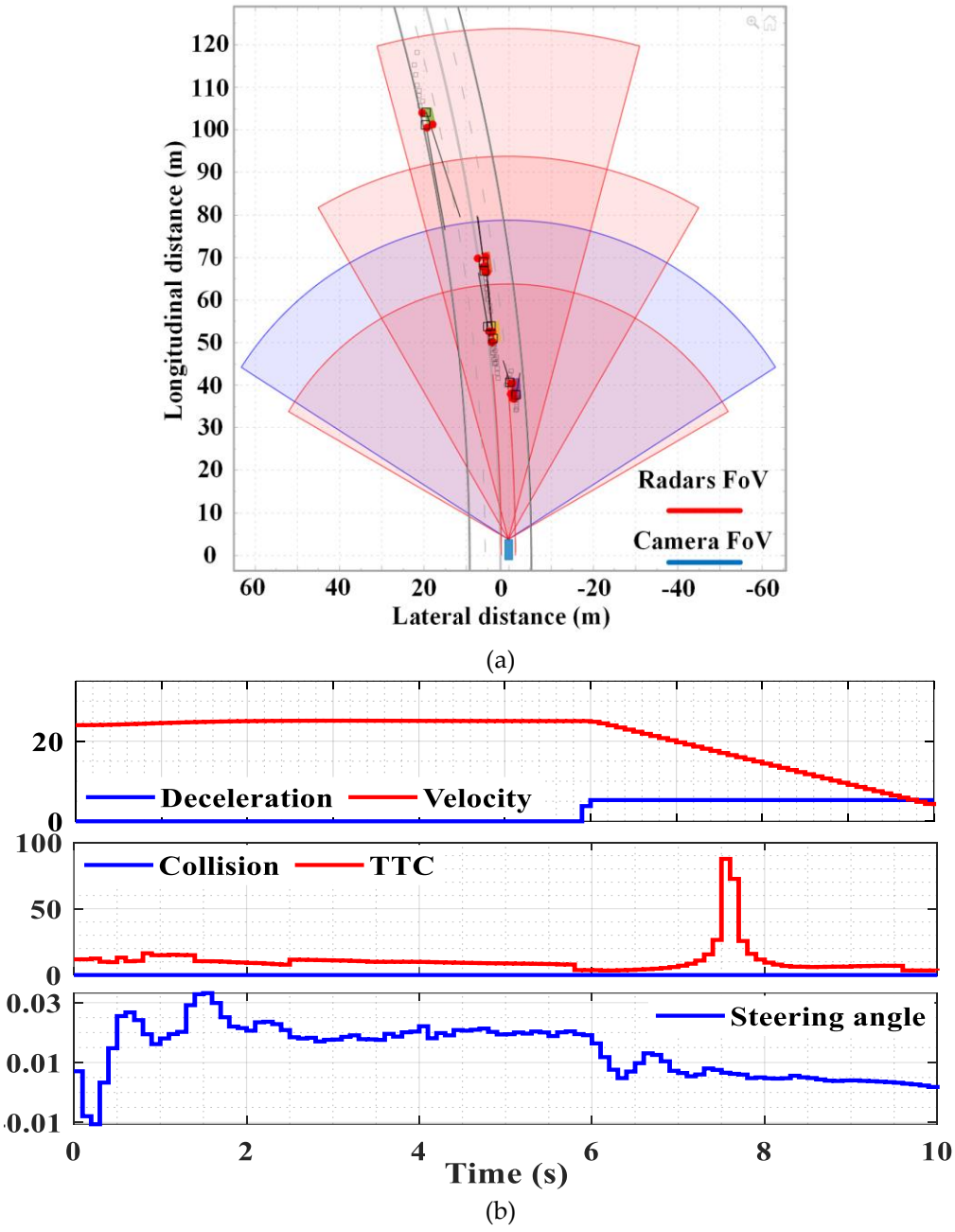

Figure 12. Performance test of proposed detection arrangement in level 2 ADAS system, (a) coordination, (b) control parameters.

Table 3. This is a table. Tables should be placed in the main text near to the first time they are cited.

 doi:10.20944/preprints202206.0323.v1

	Actor 1	Actor 2	Actor 3	Actor 4
Velocity (m/s)	15	13	25	Initially out
Initial distance (m)	138	148	162	of range

5. Conclusion

A reliable and innovative triple radar detection system for level 2 ADAS equipped vehicle is proposed in this paper. Such combination of radar sensors results in lower implementation cost and higher detection reliability, based on Based on ISO 26262 series and ISO/PAS 21448. Furthermore, the proposed multi-level radar system could operate independently of the target size and velocity and keep detection quality in bad weather conditions. The function of the proposed detection system is tested applying multiple scenarios and the performance is validated using individual subsystem and integrated systems tests. All scenarios are defined and conducted using MATLAB and Simulink (automated driving toolbox). The results demonstrated that the proposed arrangement could detect different types of targets including pedestrian, small animals and moving vehicles in different traffic scenarios. Furthermore, test results in the level 2 ADAS system revealed that the proposed arrangement of multiple radars detects the most important object even in the multiple objects presence leading to optimal operation of the AEB and LKA algorithms.

References

1. Fagnant D.J.; Kockelman K. Preparing a nation for autonomous vehicles: Opportunities, barriers, and policy recommendations. *Transp. Res. Part A: Policy and Practice* **2015,** *77*, 167.
2. Bagloee S.A.; Tavana M.; Asadi M.; Oliver T. Autonomous vehicles: challenges, opportunities, and future implications for transportation policies. J. of Mod. Transp **2016,** 24, 284.
3. Bimbraw K. Autonomous cars: Past, present and future: A review of the developments in the last century, the present scenario and the expected future of autonomous vehicle technology. In Proceedings of 12th International Conference on Informatics in Control, Automation and Robotics, Birmingham, UK, 02 March 2015.
4. Divakarla K.P.; Emadi A.; Razavi, S. A cognitive advanced driver assistance systems architecture for autonomous-capable electrified vehicles. *IEEE Trans. on Transp. Elect* **2019,** 5, 48.
5. Russakovsky O.; Deng J.; Su H.; Krause J.; Satheesh S.; Ma S.; Huang Z.; Karpathy A.; Khosla A.; Bernstein M.; Berg A.C.; Fei-Fei L. ImageNet Large Scale Visual Recognition Challenge. *Int. J. of Comp. Vis* **2015,** *115, 211.*
6. Bengler K.; Dietmayer K.; Farber B.; Maurer M.; Stiller C.; Winner H. Three decades of driver assistance systems: Review and future perspectives. *IEEE Int. Trans. Sys. Mag* **2014,** *6, 6*.
7. Campbell S.; Mahony N.; Krpalcova L.; Riordan D.; Walsh J.; Murphy A.; Ryan C. Sensor Technology in Autonomous Vehicles: A review. In Proceedings of 29th Irish Signals and Systems Conference, Belfast, UK, 2018.
8. Yang G.; Xue Y.; Meng L.; Wang P.; Shi Y.; Yang Q.; Dong Q. Survey on Autonomous Vehicle Simulation Platforms In Proceedings of 8th International Conference on Dependable Systems and Their Applications, Yinchuan, China, 05 august 2021.
9. Woo A.; Fidan B.; Melek W.W. Localization for Autonomous Driving. *Handbook of Position Location*, **2019,** 1051.
10. Haris M.; Glowacz A. Navigating an Automated Driving Vehicle via the Early Fusion of Multi-Modality. *Sensors* **2022,** 22, 1425.
11. Xu Y.; Xu D.; Lin S.; Han T.X.; Cao X.; Li X. Detection of Sudden Pedestrian Crossing for Driving Assistance Systems. *IEEE Trans. on Syst. Man Cyber* **2011,** *42, 729*.
12. Ju T.F.; Lu W.M.; Chen K.H.; Guo J.I. Vision-based moving objects detection for intelligent automobiles and a robustness enhancing method. In Proceedings of IEEE International Conference on Consumer Electronics, Las Vegas, NV, USA, 10 January 2014.
13. Ortega J. D.; Cañas P. N.; Nieto M.; Otaegui O.; Salgado L. Challenges of Large-Scale Multi-Camera Datasets for Driver Monitoring Systems. *Sensors* **2022,** *22, 2554.*
14. Bialer O.; Jonas A.; Tirer T. Super Resolution Wide Automotive Radar. *IEEE Sens. J.* **2021,** *21, 17846*.
15. Sun S.; Zhang Y.D. 4D Automotive Radar Sensing for Autonomous Vehicles: A Sparsity-Oriented Approach. *IEEE J. on Selec. Top. in Sign. Proc* **2021,** *15, 879*.
16. Chipengo U. Full Physics Simulation Study of Guardrail Radar-Returns for 77 GHz Automotive Radar Systems. *IEEE Access* **2018,** *6, 70053*.
17. Choi W. Y.; Yang J. H.; Chung Ch. Ch. Data-Driven Object Vehicle Estimation by Radar Accuracy Modeling with Weighted Interpolation. *Sensors* **2021,** *21, 2317*.
18. Ding Zh.; Sun Ch.; Zhou M.; Liu Zh.; Wu C. Intersection Vehicle Turning Control for Fully Autonomous Driving Scenarios. *Sensors* **2021,** *21, 3995*.

19. Fu Y.; Li C.; Yu F.R.; Luan T.H.; Zhang Y. A Decision-Making Strategy for Vehicle Autonomous Braking in Emergency via Deep Reinforcement Learning. *IEEE Trans. on Vehic. Tech* **2020,** *69, 5876*.
20. Bian Y.; Ding J.; Hu M.; Xu Q.; Wang J.; Li K. An Advanced Lane-Keeping Assistance System with Switchable Assistance Modes. *IEEE Trans. on Intel. Transp. Syst* **2020,** *21, 385*.
21. Guo J.; Wang J.; Luo Y.; Li K. Takagi-Sugeno Fuzzy-Based Robust H∞ Integrated Lane-Keeping and Direct Yaw Moment Controller of Unmanned Electric Vehicles. *IEEE/ASME Trans. on Mech* **2020,** *26, 2151*.
22. Tapia-Espinoza R.; Torres-Torriti M. Robust Lane Sensing and Departure Warning under Shadows and Occlusions. *Sensors* **2013,** *13, 3270*.
23. Yeong D.J.; Hernandez G.V.; Barry J.; Walsh J. Sensor and sensor fusion technology in autonomous vehicles: A review. *Sensors* **2021,** *21, 1*.
24. Kim J.; Han D.S.; Senouci B. Radar and Vision Sensor Fusion for Object Detection in Autonomous Vehicle Surroundings. In Proceedings of International Conference on Ubiquitous and Future Networks, Prague, Czechia, 03 July 2018.
25. Li W.; Wang J.; Lu L.; Wu. A Novel Scheme for DVL-Aided SINS In-Motion Alignment Using UKF Techniques. *Sensors* **2013,** *13, 1046*.
26. Hsu L. Y.; Chen T. L. Vehicle Dynamic Prediction Systems with On-Line Identification of Vehicle Parameters and Road Conditions. *Sensors* **2012,** *12, 15778*.
27. Enayati J.; Rahimnejad A.; Gadsden S. A. LED Reliability Assessment Using a Novel Monte Carlo-Based Algorithm. *IEEE Trans. on Dev. Mater. Rel* **2021,** *21, 338*.
28. Blades L.; Douglas R.; Early J.; Lo C.Y.; Best R. Advanced Driver-Assistance Systems for City Bus Applications. SAE Tech. Papers. *SAE International,* **2020,** 1.
29. Utriainen R.; Pollanen M.; Liimatainen H. The Safety Potential of Lane Keeping Assistance and Possible Actions to Improve the Potential. *IEEE Trans. on Intel Vehic* **2020,** *5, 556*.
30. Lee K.; Li S.E.; Kum D. Synthesis of robust lane keeping systems: Impact of controller and design parameters on system performance. *IEEE Trans. on Intel. Transp Syst* **2019,** *20, 3129*.